



# Stability evaluation and potential damage of a giant paleo-landslide deposit at the East Himalayan Tectonic Junction on the Southeastern margin of the Qinghai–Tibet Plateau

Yuchao Li<sup>1</sup> · Jianping Chen<sup>1</sup> · Fujun Zhou<sup>2</sup> · Zhihai Li<sup>1</sup> · Qaiser Mehmood<sup>1</sup>

Received: 9 May 2021 / Accepted: 24 November 2021 / Published online: 3 January 2022  
© The Author(s), under exclusive licence to Springer Nature B.V. 2021

## Abstract

A large number of paleo-landslide deposits exist in the Southeastern margin of the Qinghai–Tibet Plateau. Once these deposits are destroyed, the disaster chain will cause huge damage to life and property and have an impact on local geomorphic evolution. Diverse models are applied to analyze different geological problems of paleo-landslide deposits, which can produce the advantages of different models fully, thereby making up for the shortcomings of poor applicability of a single model in a certain type of problem. In this study, the Baimu paleo-landslide deposit located at the North side of Dongjiuqu Bridge of Sichuan-Tibet Railway is taken as the research object to completely analyze the potential damage by combining various technical means and numerical model, aiming to provide certain reference for the design and construction of the project. Firstly, site investigation and terrain interpretation confirm the existence of local deformation and damage. Secondly, the finite element model based on the strength reduction method is used to analyze the stability of the deposit and determine the potential damage area. For the potential damage area, debris avalanche and debris flow as two disaster transformation modes are considered. The discrete element model and shallow flow model are used to simulate the dynamic process of debris avalanche and debris flow under complex terrain, respectively. The results show that potential debris avalanche or debris flow will accumulate at the mouth of the Baimu gully, and there will be no direct threat to the bridge. Finally, the formation and evolution sequence of the deposit is proposed, which plays an important role in analyzing the evolution of local river geomorphology.

**Keywords** Paleo-landslide deposits · Stability analysis · Potential failure assessment · Numerical simulation · Landform evolution

---

✉ Jianping Chen  
chenjp@jlu.edu.cn

<sup>1</sup> College of Construction Engineering, Jilin University, Changchun 130026, China

<sup>2</sup> China Railway First Survey and Design Institute Group CO., LTD., Xi'an 710043, China

## 1 Introduction

With rapid economic growth, China's infrastructure is constantly improving. In particular, the high-speed railway network that has been continuously constructed in recent years basically covers the Eastern region, though the transportation conditions in the Western region are relatively underdeveloped. Therefore, China plans to build the Sichuan–Tibet Railway to improve transport between Sichuan and Tibet and promote the development of its Southwest region. However, the Southeastern Qinghai–Tibet Plateau presents a great obstacle to transportation construction because of its high altitude and extremely complicated geological conditions. A typical problem is the safety of railway bridges and tunnels. Affected by rapid tectonic uplift and special climate, the Qinghai–Tibet Plateau is rich in prehistoric landslides. These deposits are prone to damage under the action of rainfall or earthquakes and form various geological disasters, such as rockfalls, landslides and debris flows (Waythomas 2001; Capra and Macias 2002; Lin et al. 2003; Hurlimann et al. 2003; Cui et al. 2005). Accidents caused directly or indirectly by these disasters have occurred many times in history. For example, three large-scale debris flows occurred in the Peilong gully on the Southeast margin of the Qinghai–Tibet Plateau from 1983 to 1985. They blocked the Sichuan–Tibet Highway for 270 days and destroyed 54 bridges, causing a large amount of economic loss (Cheng et al. 2010, 2005). Flooding caused by the Yigong landslide disaster chain in 2000 reached into Palongzangbo and Brahmaputra and then into India, sweeping out structures and farmlands, interrupting traffic lines and causing inundation of the Bulamaputela River. This event claimed 94 lives and made 2.5 million people homeless (Cheng et al. 2007; Shang et al. 2003; Delaney and Evans 2015; Zhou et al. 2016). Recently, a train hit a collapsed body of a landslide and derailed at 11:40 on March 30, 2020, in Yongxing County, Hunan Province, causing 1 death and 127 injuries. These cases show that a geological disaster evaluation along the Sichuan–Tibet Railway is very important.

Many geological disaster researches in China and abroad have been focused on large-scale landslides, moraines, slump deposits, spoils, etc. (Neupane et al. 2019; Dufresne et al. 2018; Bao et al. 2019b; Shang et al. 2017). Early research on geological disasters primarily focused on the destruction mechanism and stability analysis. Geotechnical and hydrological conditions and tectonic activities are considered as prerequisites of destruction. Gravity, rainfall seepage, seismic loads and human activities can all trigger geological disasters (Li et al. 2020b; Gao et al. 2020; Yin et al. 2016; Steiakakis et al. 2009; Jarari et al. 2013). Stability analysis includes an influence factor analysis (Su and Miller 1995) and a stability calculation. For the latter, the stiffness limit equilibrium method is widely used in the early stage (Bishop 1973; Steiakakis et al. 2009; Cho and Song 2014). However, the traditional analysis method has limitations. In recent years, numerical simulations based on the finite element method (Zheng et al. 2005; Farah et al. 2011) have more often been used to calculate the slope stability after reducing the shear strength or increasing the load. In addition to the safety factor, it can reflect the stress and strain conditions during slope deformation. However, the finite element method is not ideal for analyzing large deformation problems, such as debris motion after slope failure. Traditional empirical methods (Falco et al. 2012; Fan et al. 2015) used to calculate the scope of disasters cannot consider the influence of complex geological conditions and special terrain. Therefore, the prediction of the landslide dynamic process based on numerical modeling has been a hot research topic in recent years. Discrete element models (Tang et al. 2009; Lu et al. 2014; Zhou et al. 2015; Spreafico et al. 2016; Borykov et al. 2019), smooth particle hydrodynamic models (Cuomo et al.

2016; Cascini et al. 2016; Dai and Huang 2016; Zhu et al. 2018), the finite volume shallow water flow model (Medina et al. 2008; Yavari-Ramshe et al. 2015; Han et al. 2017, 2018) and many other new methods have been applied to the simulation and prediction of geological disasters. These models can solve large deformation problems under complex conditions. Besides, discrete elements do not require complex constitutive equations; applied to the analysis of landslide movement behavior, they can intuitively reflect the microscopic mechanism under macroscopic phenomena (Lin and Lin 2015; Liu et al. 2018). Compared with discrete elements, the smooth particle hydrodynamics method and the shallow water flow model are simple to calculate and have no time-consuming features. They can be well applied to debris flow and flood simulation (Liang 2010; Ouyang et al. 2015a, b). Therefore, combined with slope stability analysis, it is of great importance to use the advantages of different numerical simulation methods to simulate the dynamic process of the potential failure and form a complete assessment.

In this study, a geological model of the Baimu paleo-landslide deposit on the Northern side of the Dongjiuqu Bridge of the Sichuan–Tibet Railway is established based on in situ surveys, geomorphic analysis and experimental data. The deposit covers 7 km<sup>2</sup>, with a volume of nearly 2 billion m<sup>3</sup>. The minimum distance between the Baimu deposit and the bridge is only 670 m. A safety assessment is urgently needed. Therefore, a finite element model is used to assess the stability and predict potential damage areas. After obtaining the potential failure zone, the discrete element model and shallow water flow model are used to simulate the movement behavior after the failure. Finally, information about the dynamic process and the disaster range is obtained and used to evaluate the external safety of the railway line.

## 2 Background

The study area is adjacent to the East Himalayan Tectonic Junction and is a typical rapid uplift region. This region is in the transitional section from the Southeast margin of the Qinghai–Tibet Plateau to the Hengduan Mountains. High ground stress, frequent earthquakes, high altitude and a significant elevation difference are typical characteristics of this region.

### 2.1 Topography and tectonic conditions

The study area is located in Lulang Town, Linzhi County, in the Southeast margin of the Tibetan Plateau (Fig. 1a, b). This region is a typical alpine-canyon landform. The topography of the Baimu paleo-landslide deposit is high and steep (Fig. 1c). The slope of the free surface is mostly inclined at 50–70° (Fig. 1d). The deposit's top platform elevation is 3490 m approximately, and the elevation of the river is 2508 m. The maximum height difference is 982 m. The long axis direction of the deposit is close to the North–South (Fig. 1e) with a length of 4100 m, and the maximum width near East–West is approximately 2400 m (Fig. 2). Horns and arêtes belonging to the glacial landform are present on the Northeast side of the mountain, and the elevation at the summit is 4714 m (Fig. 2). Judging from the topography, the total volume of the deposit exceeds 2 billion m<sup>3</sup>.

The strata developed in the study area are primarily Proterozoic Nyainqentanglha rock groups. The lithology is dominated by biotite plagioclase gneiss and biotite felsic gneiss with granite intrusion (Fig. 3a). The Baimu paleo-landslide deposit is located at the

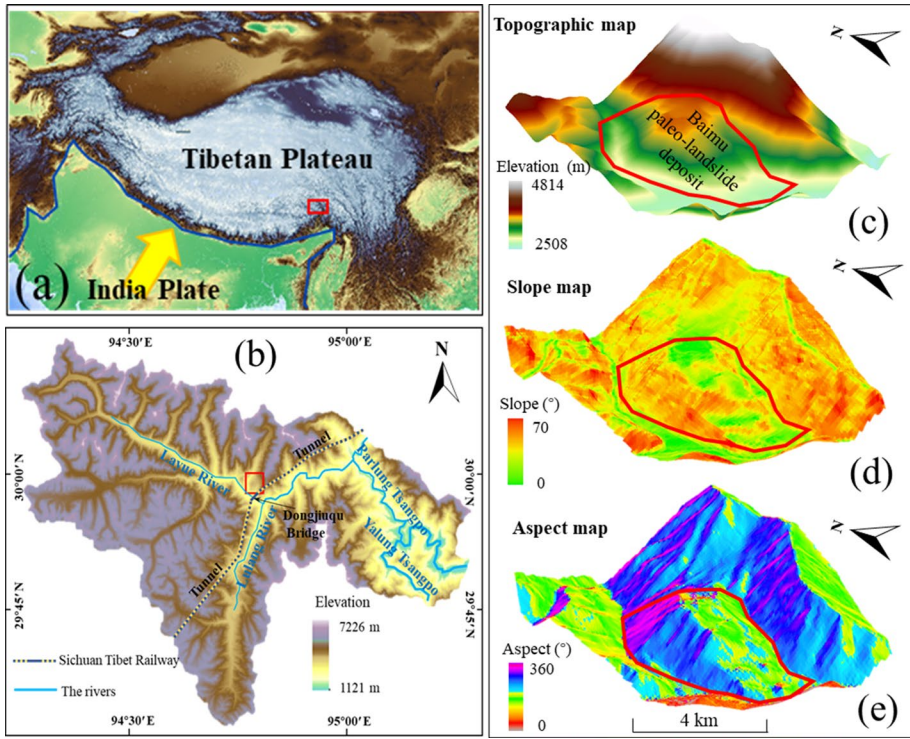


**Fig. 1** The location and terrain of the study area: **a** the Tibetan Plateau, **b** the position of the proposed railway in Lulang Town, **c** the terrain of the Baimu paleo-landslide deposit, **d** the slope of the Baimu deposit, **e** the aspect of the Baimu deposit

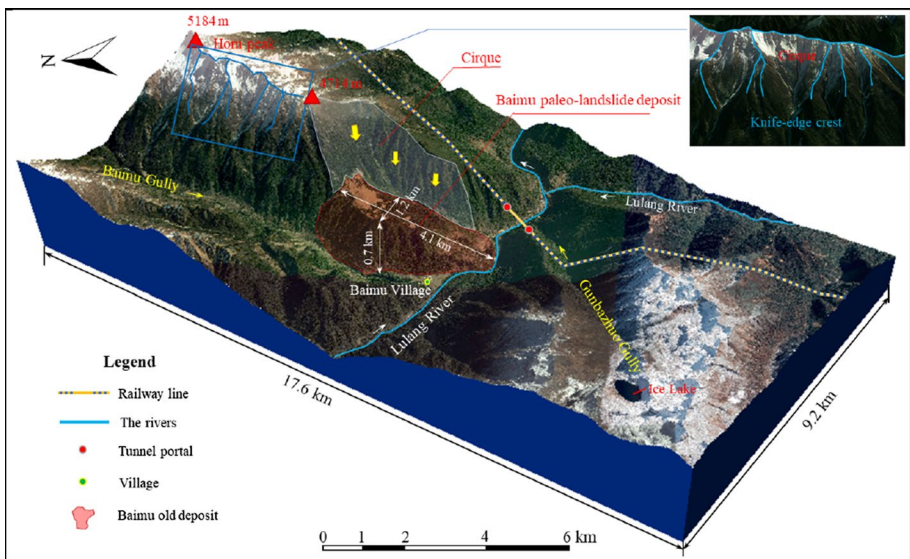


**Fig. 2** Topographic features of the Baimu paleo-landslide deposit and its surroundings

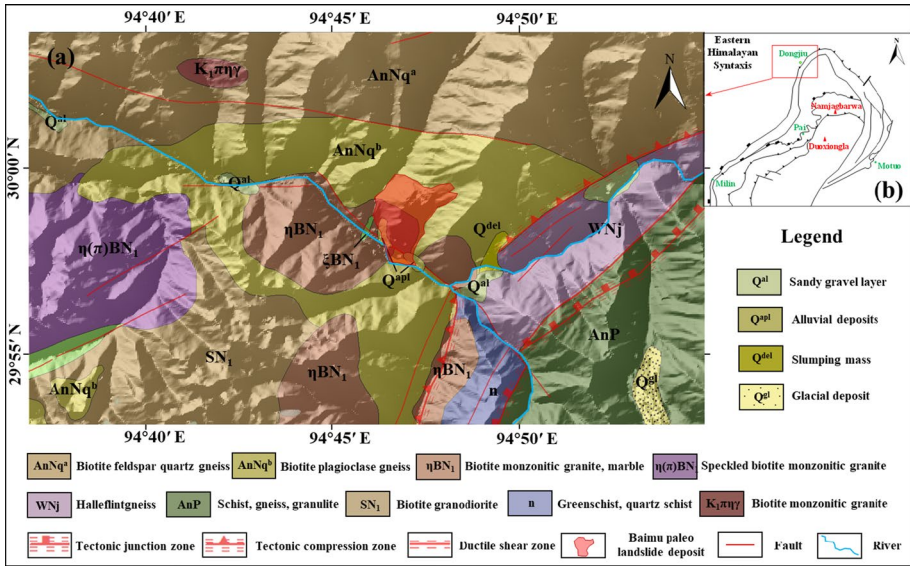


**Fig. 3** a Geological map of the study area, b East Himalayan Tectonic Junction

junction of the plaque-like biotite monzonitic granite and the biotite plagioclase granite. Affected by the East Himalayan Tectonic Junction, the geological structure of the study area is very complex (Fig. 3b). A Northeast-trending regional tectonic compression zone, ductile shear zone and tectonic junction zone are present on the Southeast side; and a Northwest trending sinistral strike slip fault develops along the Layue River.

**2.2 Rainfall condition**

The climate of the Southern and Northern foothills of the Himalayas is significantly different due to the blockage of monsoon by high-altitude mountains. Therefore, the rainfall in the study area generally shows an increasing trend with a decrease in altitude. In addition, the Namcha Barwa Peak on the SE side of the study area forms a complex topographical barrier. The river has become a natural channel for the warm and humid air from the Indian Ocean to move Northward, which further exacerbates the climatic characteristics of heavy rainfall in the study area at lower altitudes. Therefore, regions of rain and heavy rain are formed in Tongmai and Dongjiu (Fig. 4). The perennial average rainfall at the site is 1000–1500 mm, and rainfall mostly occurs from March to October, accounting for more than 90% of the total annual rainfall.

**2.3 Geological features of the Baimu paleo-landslide deposit**

Detailed field investigations were carried out to obtain the geological characteristics of the deposit. The terrain of the Baimu paleo-landslide deposit remains obviously inconsistent with the surroundings (Fig. 5a). This feature is a result of epigenetic superficial geological reformation. The top platform of the deposit presents a wavy terrain (Fig. 5b), and it alternates from

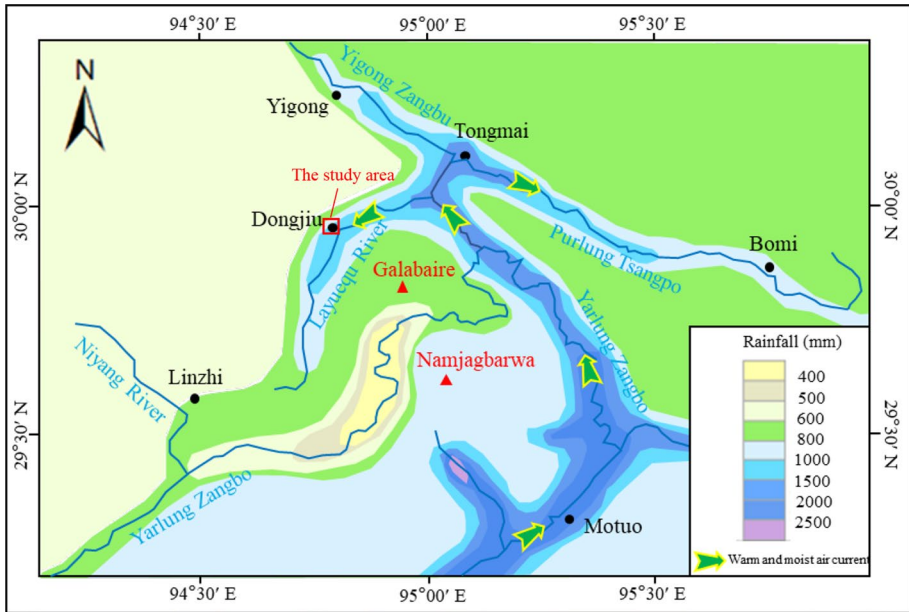


**Fig. 4** Distribution map of average annual rainfall in the study area

South to North three times with an undulating slope of 5–14°. The formation of the wavy terrain is related to the difference in velocity between different parts during motion.

Figure 5c, d shows the outcrop characteristics at different locations of the deposit. The deposit is primarily composed of granitic gneiss debris of different size mixed with sand and soil. The debris is primarily angular and subangular in poor sorting. The consolidation of the deposit is good, but the strength is uneven. Rockfalls and landslides occur at the Northern side of the platform affected by erosion (Fig. 5e). Continuous bedrock outcrops ca. 1.2 km long and about 250 m wide are at the Southern edge of the Baimu paleo-landslide deposit. The fresh and intact bedrock here plays a role of a natural retaining wall (Fig. 5f), effectively preventing the potential destruction on the South side of the deposit.

Affected by weathering, unloading, rainfall erosion and seismicity, small-scale damages are common in the Western side of the deposit (Fig. 6a). These unfavorable geological phenomena, rockfalls (Fig. 6b) and landslides (Fig. 6c) mainly, occur at the lower parts of the slopes. Therefore, loose deposits are continuously distributed at the foot of the slope on the West side of the Baimu deposit (Fig. 6d).

Due to the huge scale (the maximum thickness reaches approximately 400 m) (Fig. 6e) and the obvious local damage of the Baimu paleo-landslide deposit, it is necessary to analyze its stability and potential failure. This study uses different methods and models to address different geological problems. The flow chart from data collection and processing to model establishment and calculation is shown in Fig. 7.

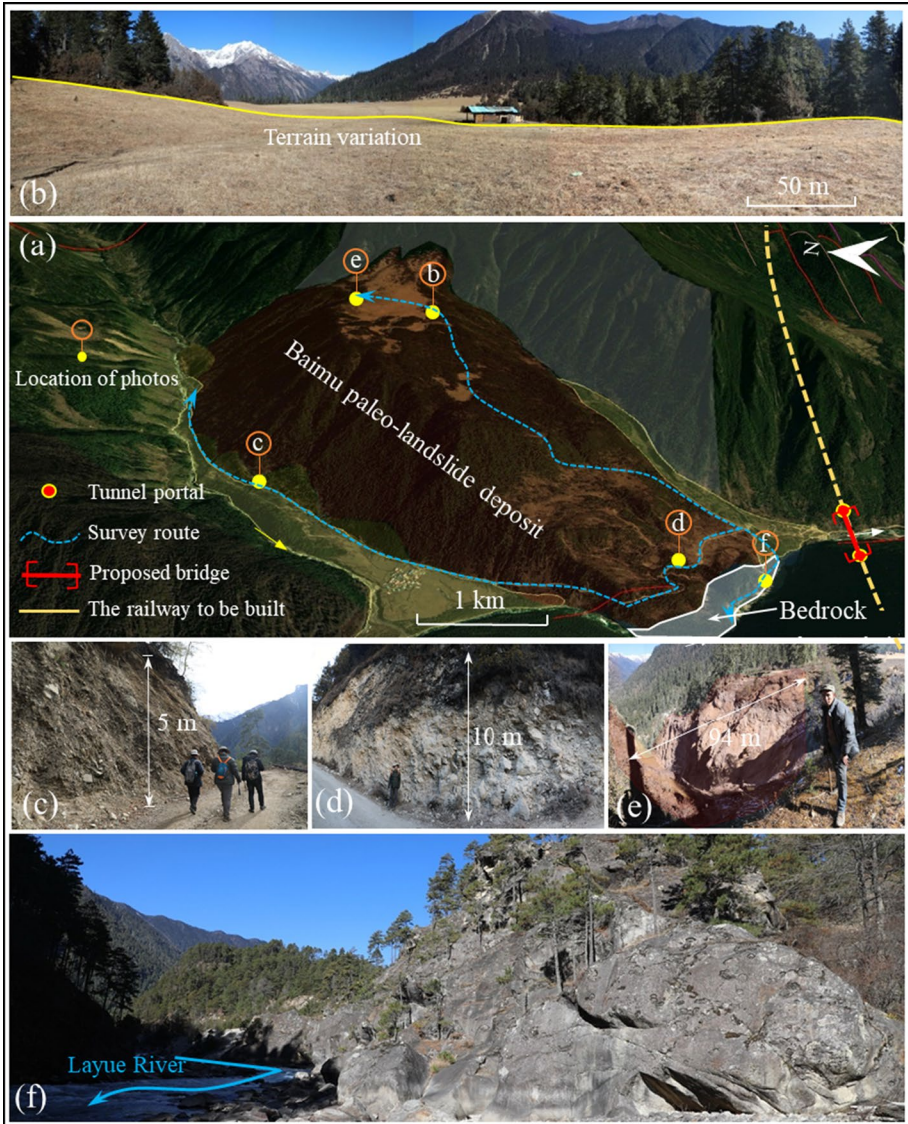


**Fig. 5** Photographs of the Baimu paleo-landslide deposit: **a** survey route and photograph location, **b** wavy platform at the top, **c** outcrop on the West side, **d** outcrop on the South side, **e** phenomenon of local collapse, **f** bedrock outcrop at the Southern side of the deposit close to the river

### 3 Stability analysis and failure area estimation

The stability assessment of the Baimu paleo-landslide deposit depends on the finite element model (ABAQUS). The strength reduction method is used to analyze the stress–strain state and then calculate the plastic zone and safety factor. The actual shear strength  $C$  and  $\varphi$  are discounted into  $C_R$  and  $\varphi_R$  using a strength reduction factor (SRF). The new shear strength parameters  $C_R$  and  $\varphi_R$  are used for the calculation until the slope reaches a

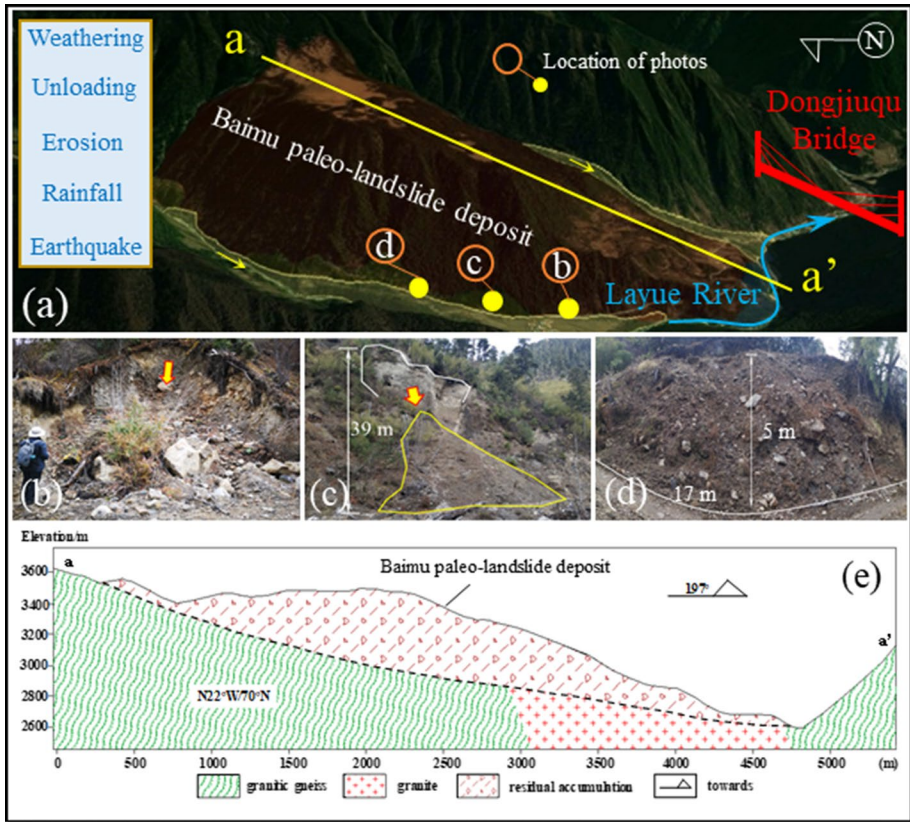


**Fig. 6** a Image and typical outcrop location of the Baimu paleo-landslide deposit, b local collapses, c local landslide, d loose deposit, e longitudinal profile of the deposit

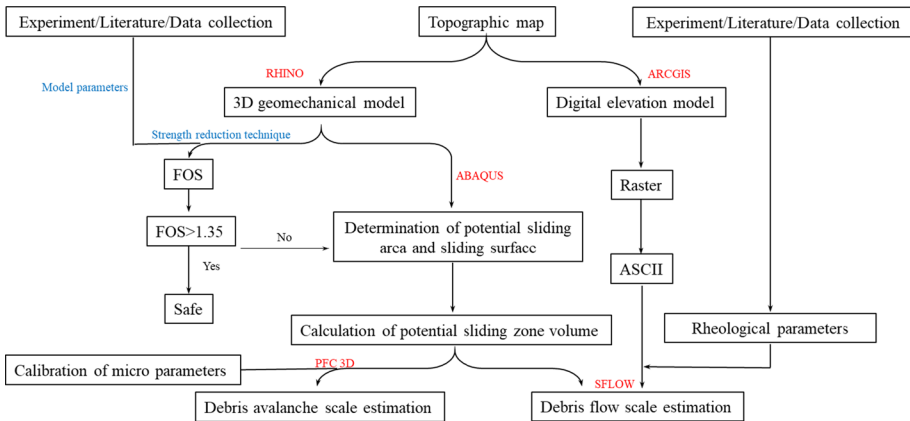


**Fig. 7** Research flow chart. According to the technical code for building slope engineering (GB50330-2013), considering the importance of slope to engineering safety and the influence of various geological factors on stability, the safety factor is set as 1.35 to keep enough safety reserves



limit failure state, and the SRF is equal to the factor of safety (FOS). The method can be expressed as Eqs. (1) and (2). The strength reduction technique is performed by defining the field variables in ABAQUS (Bao et al. 2019b).

$$\frac{\int \left( \frac{c}{K} + \frac{\sigma}{K} \tan \varphi \right) dA}{\int \tau dA} = \frac{\int (c_R + \sigma \tan \varphi_R) dA}{\int \tau dA} = 1 \tag{1}$$

$$c_R = \frac{c}{K} \varphi_R = \arccot \left( \frac{\tan \varphi}{K} \right) \tag{2}$$

### 3.1 Model processing

The digital elevation model is processed into a 3D contour and imported into the modeling software Rhino to create a 3D geomechanical model. The model can be directly imported into ABAQUS software for calculation. During the on-site investigation, no obvious cracks are found; the deposit can be regarded as a whole. The model primarily involves two kinds of material whose boundaries are mainly defined by the transverse, longitudinal and main sliding-direction profiles (Fig. 8a–c). The boundary conditions of the model are set as follows: the surface of the slope body is not limited and can be deformed freely; the surrounding walls are not deformable in the normal direction, and the other directions are free; the bottom surface is set as a fixed surface and cannot be deformed (Fig. 8d). When meshing, considering the calculation efficiency and calculation accuracy, the model is divided into tetrahedral meshes (Fig. 8e).

In the simulation process, M-C strength criterion is chosen as the constitutive model. In addition, several material parameters are necessary, including the density  $\rho$ , cohesion

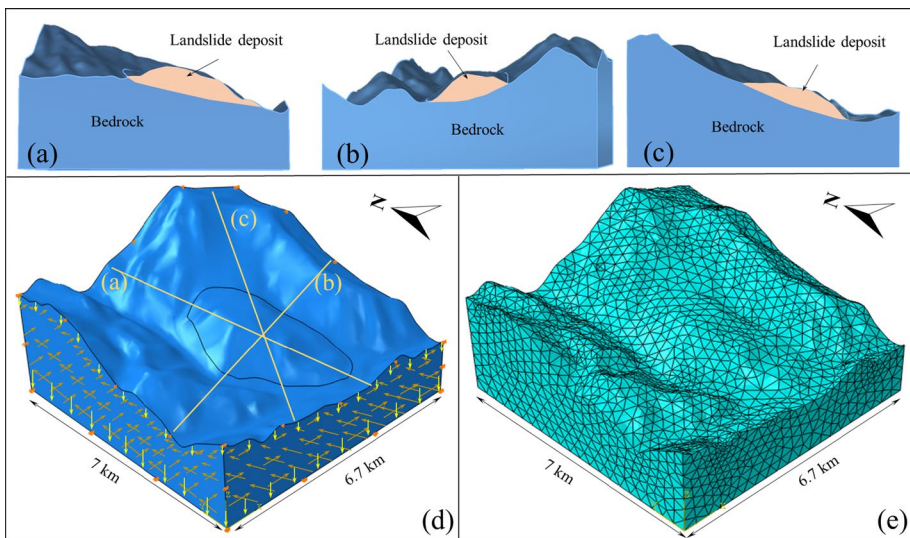


**Fig. 8** **a** Longitudinal profile of the model, **b** cross profile of the model, **c** main sliding-direction profile of the model, **d** boundary conditions of the 3D model, **e** model meshing

$C$ , internal angle of friction  $\varphi$ , Poisson’s ratio  $u$  and elasticity modulus  $E$ . The selection of calculation parameters is primarily based on the field measurements, laboratory tests and previous summary of the physical parameters of the deposits near the study area (Geng 2015). For the bedrock, these values are taken as  $\rho = 2.65 \text{ g/cm}^3$ ,  $C = 24 \text{ MPa}$ ,  $\varphi = 53^\circ$ ,  $u = 0.18$  and  $E = 33 \text{ GPa}$ . For the paleo-landslide deposit, this study summarizes the previous experimental studies on the physical and mechanical parameters of typical landslide deposits in Southeastern Tibet where ten deposits belong to the same watershed as the Baimu deposit (Fig. 9a), and their geological characteristics are similar (Fig. 9b). The important parameters of the elastic modulus, Poisson’s ratio, density, internal friction angle and cohesion are used to draw the fitting curve (Fig. 9c). The results show that the physical and mechanical parameters of the paleo-landslide deposits at different positions are similar and only fluctuate in a relatively stable, small range. As the shear strength parameters have the greatest impact on stability, we discuss the influence of the upper and lower limits of the two parameters, cohesion ( $C : 64\text{--}82 \text{ kPa}$ ) and internal friction angle ( $\varphi : 29\text{--}38^\circ$ ), on the research results. The rest of the parameters take the mean of the distribution ( $\rho = 2.14 \text{ g/cm}^3$ ,  $u = 0.24$ , and  $E = 47 \text{ MPa}$ ) according to the fitting curve.

Three main failure criteria are applied to judging the slope failure in the calculation of the finite element model (Bao et al. 2019b): (1) the convergence criterion, (2) the penetration criteria of the plastic deformation zone and (3) the displacement catastrophe principle. This study uses the plastic deformation zone penetration criterion, which is judged by the change and distribution of the generalized shear strain and other physical quantities in the domain. This criterion is met when the plastic zone in the domain is connected.

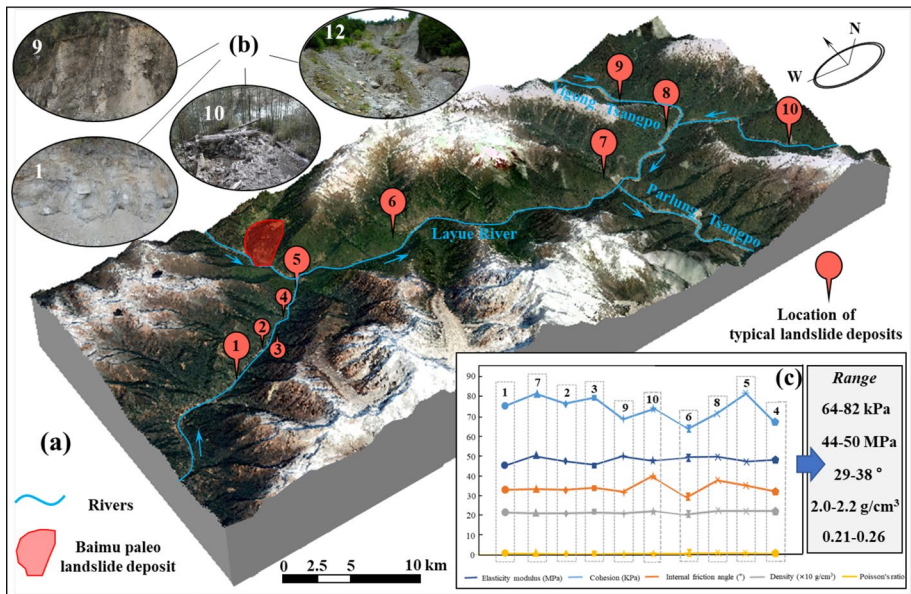


**Fig. 9** a Distribution of typical landslide deposits in the study area, b photographs of typical deposits, c curves of physical and mechanical parameters of typical landslide deposits

### 3.2 Simulation results

The results of the stability analysis show that with the continuous decrease of strength parameters, the deformation zone (Fig. 10) is formed at the Southwestern part of the Baimu paleo-landslide deposit. When the initial shear strength parameters ( $C, \varphi$ ) are set to the maximum value, the FOS is 1.31, and the area of the deformation zone is about 0.76 km<sup>2</sup> (Fig. 10a, b). When the initial shear strength parameters are set to the minimum value, the FOS is 1.24, and the deformation zone increases slightly up to the area of 0.8 km<sup>2</sup> and the thickness of about 130 m (Fig. 10c, d). According to “The technical code for building slope engineering (GB50330-2013) (2013)”, when the FOS < 1.35, the slope is considered not very stable. The scale of potential damage in the most dangerous situation (the largest potential damage zone) is our concern. Therefore, the range of deformation zone with minimum shear strength parameters (Fig. 10e) will be used as the direct basis for the numerical simulation of potential failure.

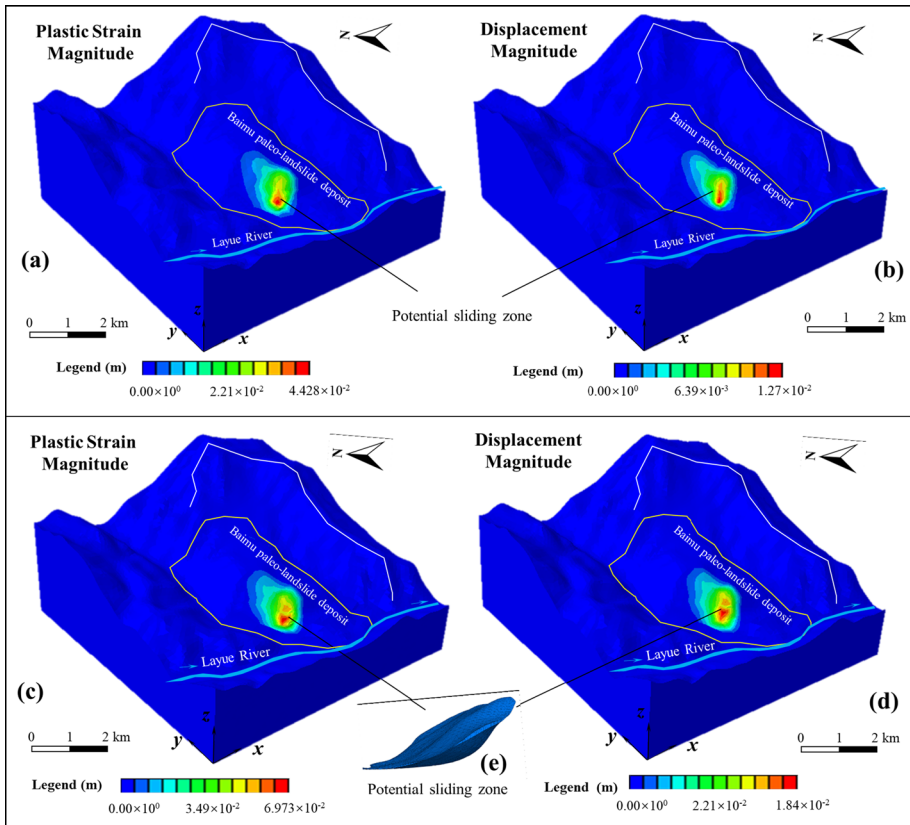


**Fig. 10** Stability analysis: **a** plastic zone diagram when the shear strength parameters take the maximum value, **b** displacement diagram when the shear strength parameters take the maximum value, **c** plastic zone diagram when the shear strength parameters take the minimum value, **d** displacement diagram when the shear strength parameters take the minimum value, **e** potential failure zone

## 4 Numerical simulation of potential failure

For the potential failure area determined by the stability analysis, we think that there are two main modes of failure (debris avalanche or debris flow) under the action of self-weight stress, an earthquake or rainstorm. For the potential debris avalanche and debris flow, PFC3D (Cundall and Strack 1979) software based on the discrete element model and SFLOW software (Han et al. 2017) based on the shallow water flow model, respectively, are used to perform the simulation.

### 4.1 Debris avalanche simulation

The macroscopic material properties of the PFC model, such as Young's modulus and Poisson's ratio, can be obtained from the interaction of particles and bonds by setting microscopic properties:

$$\{E_c, (kn/ks), \mu\}, \text{ microscopic properties of particles;}$$

$$\{\lambda, \bar{E}_c, \left(\frac{\bar{k}_n}{\bar{k}_s}\right), \bar{\sigma}_c, \bar{\tau}_c\}, \text{ microscopic properties of bonds,}$$

here,  $E_c$  and  $\bar{E}_c$  indicate the modulus of the particle and bond, respectively;  $(kn/ks)$  and  $\left(\frac{\bar{k}_n}{\bar{k}_s}\right)$  are the ratio of normal to shear stiffness of the particle and bond, respectively;  $\mu$  is the particle friction coefficient;  $\lambda$  is the radius multiplier used to set the parallel-bond radii (which can transmit forces and moments between particles); and  $\sigma_c$  and  $\tau_c$  are the normal and shear strengths of the bonds, respectively. The modulus of the particle and parallel bond can be expressed as follows:  $E_c = k_n/4R$  and  $\bar{E}_c = \bar{k}_n(R_1 + R_2)$ , where  $R$  is the radius of the particles (Potyondy and Cundall 2004; Itasca 2008). The macroscopic parameters of the Baimu paleo-landslide deposit ( $\rho$ ,  $C$ ,  $\varphi$ ,  $u$  and  $E$ ) have been determined in the Sect. 3. Therefore, the triaxial compression experimental model is used to calibrate the microscopic parameters of particles and bonding (Fig. 11). The macro parameters of the material are calculated by continuously adjusting the micro parameters until the calibration results are consistent with the known physical and mechanical parameters (Table 1).

In numerical compression test, the range of particle size is usually set to a small value to simulate laboratory test. However, to prevent excessive calculations and data overloading in numerical simulations of PFC 3D, the range of particle size should be enlarged in the numerical landslide model (Lu et al. 2014; Lin and Lin 2015). Enlarging the particle radius will affect some microscopic parameters. As particle contact modulus ( $E_c$ ) and parallel bond modulus ( $\bar{E}_c$ ) are inversely proportional to particle radius, these two parameters have to be reduced by the same multiple when the particle radius is enlarged in the actual simulation (Bao et al. 2020; Lu et al. 2014; Lin and Lin 2015). However, the influence of particle radius on bond strength and friction coefficient is unknown and cannot be expressed by simple numerical scaling; in practice, it is often necessary to discuss the rationality of the results through trial calculations of parameter sensitivity. Based on the calibration results of the compression experimental model, we set four levels of friction coefficient ( $f$ ) and normal bond strength ( $\sigma_c$ ) (shear bond strength is one third of normal bond strength) between particles to discuss the simulation results, i.e.,  $f=0.1, 0.13, 0.16$  and  $0.2$ ;  $\sigma_c=0.05, 0.10, 0.15$  and  $0.20$  MPa. The results show that the migration distance and accumulation scale of debris avalanche decrease

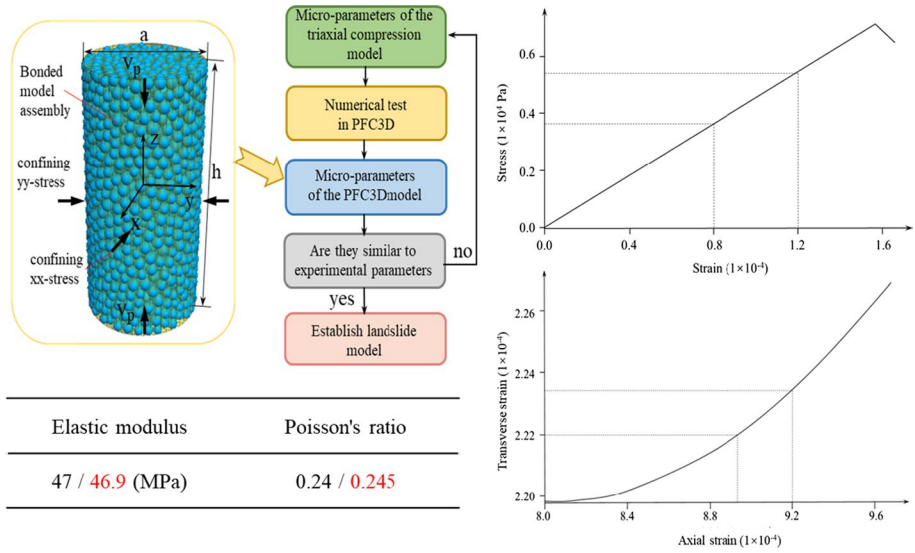
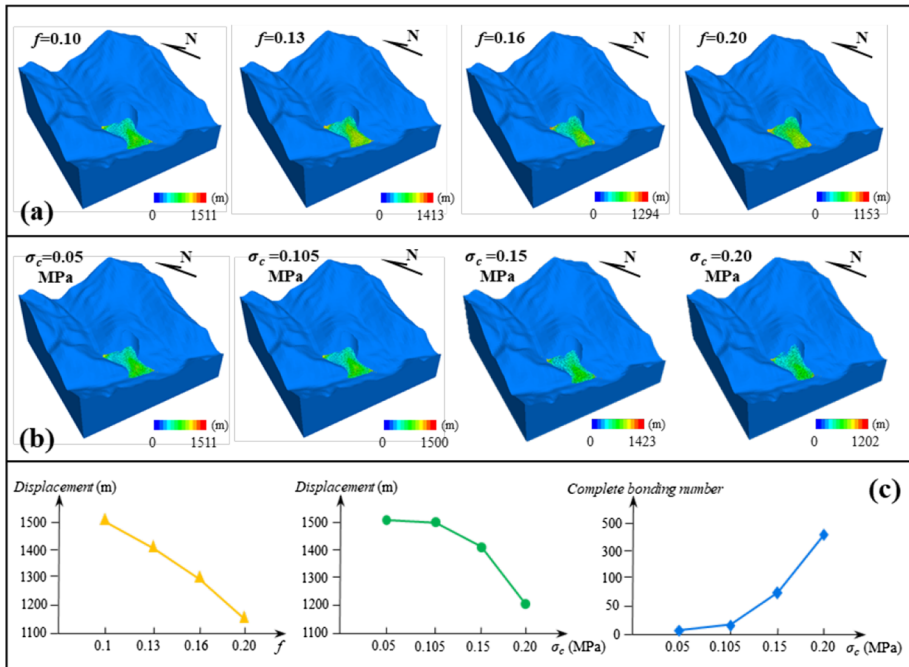


Fig. 11 Calibration of microscopic parameters of discrete element model

Table 1 PFC3D model calculation parameters

| Properties of PFC model                            | Simulation parameters of compression experiment | Calculation parameters |
|--|---|------------------------|
| Minimum particle size ( $r_{min}$ ) (m)            | 0.06  | 6                      |
| Ball particle density ( $kg/m^3$ )                 | 2150  | 2150                   |
| Ball stiffness ratio (pb_krat) (kn/ks)             | 2   | 2                      |
| Ball-ball friction coefficient (fric)              | 0.13  | 0.1                    |
| Friction angle ( $^\circ$ )                        | 33  | 33                     |
| Particle contact modulus ( $E_c$ ) (GPa)           | 26  | 0.26                   |
| Parallel bond modulus (pb_ $E_c$ ) (GPa)           | 26  | 0.26                   |
| Parallel bond stiffness ratio (pb_krat) (kn/ks)    | 2   | 2                      |
| Parallel bond normal strength ( $\sigma_c$ ) (MPa) | 0.105   | 0.10                   |
| Parallel bond shear strength ( $\tau_c$ ) (MPa)    | 0.035   | 0.033                  |

obviously with the increase of friction coefficient (Fig. 12a, c). The variation of bond strength has similar laws (Fig. 12b): when the bond strength is less than 0.10 MPa, the migration distance and accumulation range of debris avalanche are basically unchanged (Fig. 12c), indicating that there is almost no complete bond in the deposit; when the bond strength is greater than 0.10 MPa, the number of complete bonds in the debris avalanche deposit increases significantly, resulting in a significant reduction in the migration distance (Fig. 12c). In addition, considering that the actual bond strength is smaller than the calibration value of the compression model and the collision during the sliding process will make the particles and the wall smooth, in the numerical simulation, the calculated values of friction coefficient and bond strength should be slightly lower than the calibrated values of the compression model. And we are concerned about the dangerous situation with the largest disaster range. Therefore, the final calculated values of



**Fig. 12** a Accumulation range of debris avalanche under different friction coefficients, b accumulation range of debris avalanche under different bond strength, c influence of friction coefficient and bond strength on the displacement of debris avalanche and the complete bond quantity in the deposit

friction coefficient and bond strength in the simulation are 0.1 and 0.10 MPa, respectively (Table 1).

The numerical simulation results of the debris avalanche show that the sliding duration is 30 s (Fig. 13). The maximum movement distance of the debris avalanche is 1.5 km (Fig. 13a). In the process of movement, the velocity of the particles is generally 15–25 m/s (Fig. 13b), and the maximum velocity of individual particles is 40 m/s. Finally, the debris avalanche primarily accumulated at the mouth of the Baimu gully.

The accumulation characteristics are analyzed by setting section lines at typical locations of the debris avalanche (Fig. 14a). The accumulation length of the debris avalanche along the Baimu gully is approximately 1.3 km. The maximum stacking thickness is 150 m (Fig. 14b). The accumulation length along the Layue River is approximately 0.7 km, and the accumulation thickness is 60–75 m. The debris avalanche will block the Layue River (Fig. 14c).

## 4.2 Debris flow simulation

SFLOW based on the finite volume shallow flow model (Ouyang et al. 2013) can effectively consider the bottom friction and energy conversion in the movement process, and it has a good effect in the simulation of debris flow under complex terrain (Han et al. 2018). In a SFLOW model, rheological parameters of potential debris flows reflecting physical and rheological properties are needed. The rheological parameters  $\alpha_1$ ,  $\alpha_2$ ,  $\beta_1$ ,  $\beta_2$  are empirical, and they

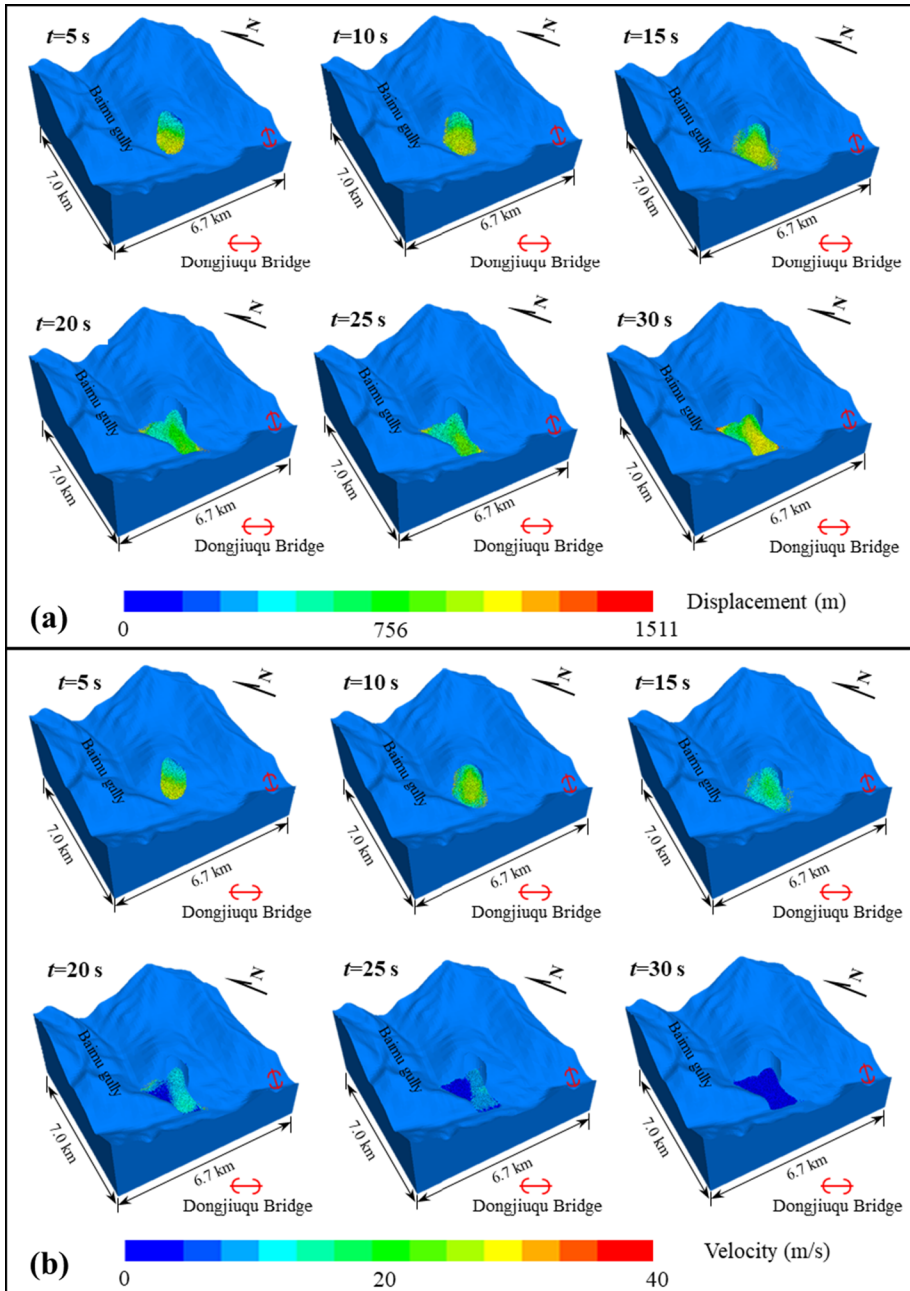


**Fig. 13** Displacement and velocity nephogram of the debris avalanche at different times in the simulation

are determined according to the suggestions of FLO-2D User’s manual and previous typical debris flow research (O’Brien 2006; Bao et al. 2019a; Li et al. 2021a). Considering the vegetation conditions in the study area, the resistance coefficient ( $K$ ) is selected as 2500, which has

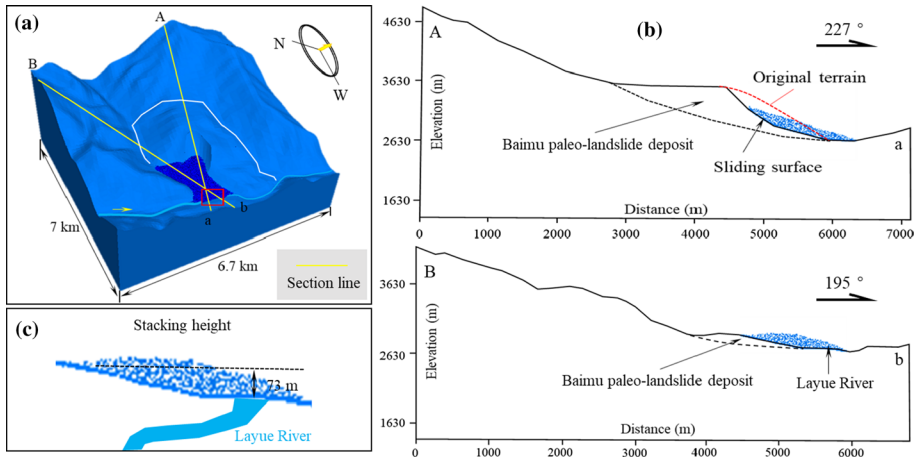


**Fig. 14** **a** 3D model of the debris avalanche deposit, **b** two typical sections of the debris avalanche deposit, **c** height of blocking the river

been used effectively for many mudflow events (Li et al. 2021b; Chen et al. 2017; Han et al. 2017). The Manning’s coefficient ( $n$ ) used is 0.2 according to previous studies (Li et al. 2021b; Chang et al. 2017; Chen et al. 2017). The parameter  $C_v$  for debris flow is calculated as 0.533 when the density of water ( $\rho_w$ ) is 1000 kg/m<sup>3</sup>, the density of sediment mixture ( $\rho_m$ ) is 2500 kg/m<sup>3</sup>, and the debris flow density is 1800 kg/m<sup>3</sup> (DZ/T0220 2006; Bao et al. 2019a; Li et al. 2021a). The reference values of rheological parameters are shown in Table 2.

In numerical simulation, debris flow volume and hydrograph are important. The hydrograph includes two parts: the time of debris flow movement process and the discharge at different times. For debris flow, its scale depends on rainfall intensity and duration. In this study, the flood hydrographs are calculated based on empirical formulas (Eq. 3–7) recommended by the China Institute of Water Resources and Hydropower, “Specifications for Geological Investigation of Debris Flows Stabilization (DZ/T0220–2006)”, and “The Rainstorm and Flood Calculation Manual of Medium and Small Basins in Sichuan Province”, for 20, 50, 100 and 200-year return periods (Chang et al. 2017).

$$Q_m = 0.278fiF = 0.278\varphi \frac{S_p}{t^n} F \tag{3}$$

$$W_p = 0.1h_R F \tag{4}$$

$$T_p = 0.278 \left( \frac{W_p}{Q_m} \right) \tag{5}$$

$$T = B_F T_p \tag{6}$$

$$Q_c = Q_m (1 + \varphi_1) D \tag{7}$$

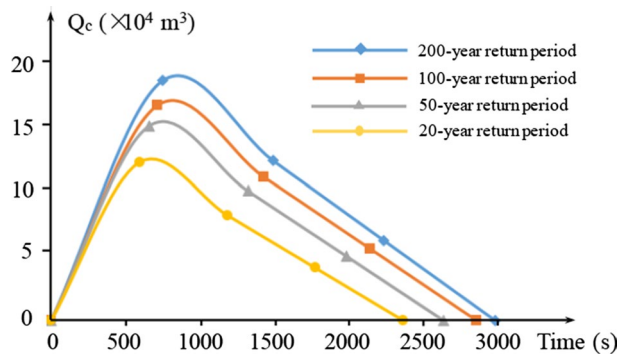


**Table 2** List of reference values for rheological parameters

| Source                                      | $\eta = \alpha_1 \exp(\beta_1 \cdot C_v)$   |           | $\tau = \alpha_2 \exp(\beta_2 \cdot C_v)$ |  | References  |
|---|---|-----------|---|--|---|
|   | $\alpha_1$                                  | $\beta_1$ | $\alpha_2$                                | $\beta_2$  |   |
| $\alpha_1, \alpha_2, \beta_1, \beta_2$      |   |           |   |  |   |
| FLO-2D User's manual case                   | 0.811                                       | 13.72     | 0.00462                                   | 11.24  | Bao et al. (2019a)<br>O'Brien (2006)<br>Li et al. (2021a) |
| Case  | Gully surface                               |           | Value                                     | References   |   |
| $K$   |   |           |   |  |   |
| Peilong gully, Tibet                        | Good vegetation                             |           | 2500                                      | Li et al. (2021b)  |   |
| Xiaojia gully, Sichuan                      | Sparse vegetation                           |           | 2500                                      | Chen et al. (2017)   |   |
| Xiaojia gully, Sichuan                      | Sparse vegetation                           |           | 2500                                      | Han et al. (2017)  |   |
| Longxihe basin, Sichuan                     | Sparse vegetation                           |           | 2285                                      | Chang et al. (2017)  |   |
| $N$   |   |           |   |  |   |
| Peilong gully, Tibet                        | Good vegetation                             |           | 0.32                                      | Li et al. (2021b)  |   |
| Xiaojia gully, Sichuan                      | Sparse vegetation                           |           | 0.16                                      | Chen et al. (2017)   |   |
| Xiaojia gully, Sichuan                      | Sparse vegetation                           |           | 0.05                                      | Han et al. (2017)  |   |
| Longxihe basin, Sichuan                     | Sparse vegetation                           |           | 0.07                                      | Chang et al. (2017)  |   |
| Source                                      | $f = (\rho_n - \rho_w) / (\rho_m - \rho_n)$ |           | $C_v = (1 + f) / f$                       | References   |   |
|   | $\rho_w$                                    | $\rho_n$  | $\rho_m$                                  |  |   |
| $C_v, \rho_w, \rho_n, \rho_m$               |   |           |   |  |   |
| Specification and debris flow research case | 1000  | 1800      | 2500                                      | DZ/T0220 (2006)<br>Bao et al. (2019a)<br>Li et al. (2021a) |   |

where  $Q_m$  is the clear water peak at different frequencies ( $m^3/s$ );  $t$  is the confluence time (h);  $\varphi$  is the flood peak runoff coefficient;  $S$  is the storm intensity (mm/h);  $n$  is the rain-storm formula index; and  $F$  is the watershed area ( $km^2$ );  $W_p$  is the total design flood;  $T_p$  is the duration of the flood process;  $B_F$  ( $1/(1 - C_v)$ ) is the expansion coefficient;  $T$  is the duration of debris flow;  $Q_c$  is the peak flow of debris flow. The correction coefficient  $\varphi_1$  and

**Fig. 15** Hydrographs of debris flows for different return periods



the clogging coefficient  $D$  are obtained from the empirical formula. The final determined hydrographs of debris flow are shown in Fig. 15.

The simulation results (Fig. 16) show that the simulated range of debris flow of the 20-year return period is basically identical to the present accumulation range of debris flow in the gully mouth (Fig. 16a). The maximum accumulation thickness is 42 m. As the frequency of debris flow decreases, the accumulation range and scale increase significantly (Fig. 16b, c). For the 200-year return period, the maximum stacking thickness is 59 m, and the stacking length is 2 km along the Layue River (Fig. 16d).

## 5 Discussion

### 5.1 Comprehensive analysis

The Baimu paleo-landslide deposit is located in the rainy canyon area adjacent to the Eastern Himalayan Tectonic Junction with an annual average rainfall of more than 1000 mm and frequent earthquakes. Some typical rock outcrops show signs of earthquake action, and several landslides on the surface of the deposit are also related to rainfall erosion (Fig. 6b, c). The South side of the Baimu paleo-landslide deposit is the planned construction site for the Dongjiuqu Bridge of the Sichuan–Tibet Railway. Therefore, the stability of the deposit and the dynamic process of the potential failure are directly related to engineering safety. The overall stability of the Baimu paleo-landslide deposit can be considered good according to the finite element model analysis. However, the Southwest side of the deposit is prone to local instability, which may cause debris avalanches or debris flows. Due to the special climatic and structural conditions in the study area (Figs. 3, 4), intense rainfall

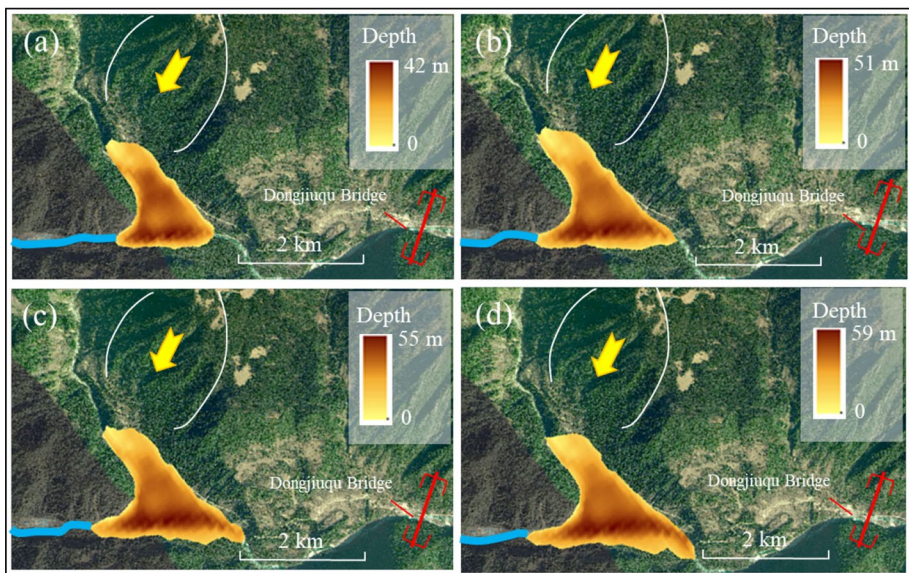


**Fig. 16** Disaster range of debris flows for different return periods: **a** 20-year return period, **b** 50-year return period, **c** 100-year return period, **d** 200-year return period

erosion and frequent seismic activity are the most likely triggers for the deposit destruction. The finite element model has been successfully applied in a large number of nonlinear stability analysis problems (Wang et al. 2015; Xiao et al. 2016; Bordoni et al. 2015; Khan et al. 2017) and determined the potential failure area of the Baimu deposit. But it can't simulate large deformation problems, especially the sliding process. The discrete element software PFC equates the debris avalanche as a particle flow model and replaces the interaction between rock and soil with the bond between particles. It can simulate the dynamic process of debris avalanche under complex terrain conditions (Bao et al. 2020). Motion characteristics such as velocity and displacement can be easily obtained (Poisel and Roth 2004; Poisel et al. 2005). And the interaction between particles can also be well reflected (Tang et al. 2009, 2013; Lo et al. 2011; Zhou et al. 2015). As far as pure discrete element model is obviously not suitable for the special water–solid coupling material such as debris flow, the SFLOW based on shallow water flow model is used to simulate such phenomena. The model is based on the principle of fluid continuous motion and mass conservation, which can be used to simulate the whole process of debris flow (Han et al. 2017, 2018). In addition, the model considers not only the complex terrain conditions, but also the friction properties at the bottom of the fluid, the viscosity properties and the contact energy loss of solid particles. This study uses a variety of numerical models to realize the disaster chain analysis from the stability of the deposit to the potential destruction, which is of great significance for the prevention and control of potential disasters of large-scale paleo-landslide deposits.

## 5.2 Disaster range analysis

In the case of Baimu paleo-landslide deposit, the discrete element model and shallow water flow model are used to simulate the dynamic processes of debris avalanches and debris flows, respectively. The results show that once a debris avalanche or debris flow occurs, most of it will accumulate in the mouth of the Baimu gully. The largest disaster range was found for the 200-year return period debris flow, though the minimum distance to the proposed bridge would be 1.6 km (Fig. 17a), thus there will be no direct threat to this structure. However, debris avalanche or debris flow can cause river blocking. Once a dam breaks, floods will form. The proposed bridge is designed without a pier, and the clear space under the bridge is up to 200 m (Fig. 17b) so that the possibility of flood impact is effectively avoided.

The maximum thickness of the debris avalanche dam formed by the destruction of the deposit in the Layue River is 73 m (Fig. 14c), which means that the blocking of the river may cause the water level of the Layue River to rise by more than 70 m. Such a huge storage capacity, once the dam body collapses, will be a devastating blow to downstream residents and infrastructure. For example, in October and November 2018, large-scale high-level landslides occurred in Baige, Tibet, which caused river blockage. A flood formed after the dam broke, destroying several houses, roads and bridges (Li et al. 2020a; Hu et al. 2020; Gan et al. 2020). The analysis of the dam-break flood caused by the landslide will be the focus of future research.

## 5.3 Landform evolution

Based on the study of the disaster chain of Baimu paleo-landslide deposit, we propose a universally significant evolutionary sequence of giant paleo deposits on the Southeastern

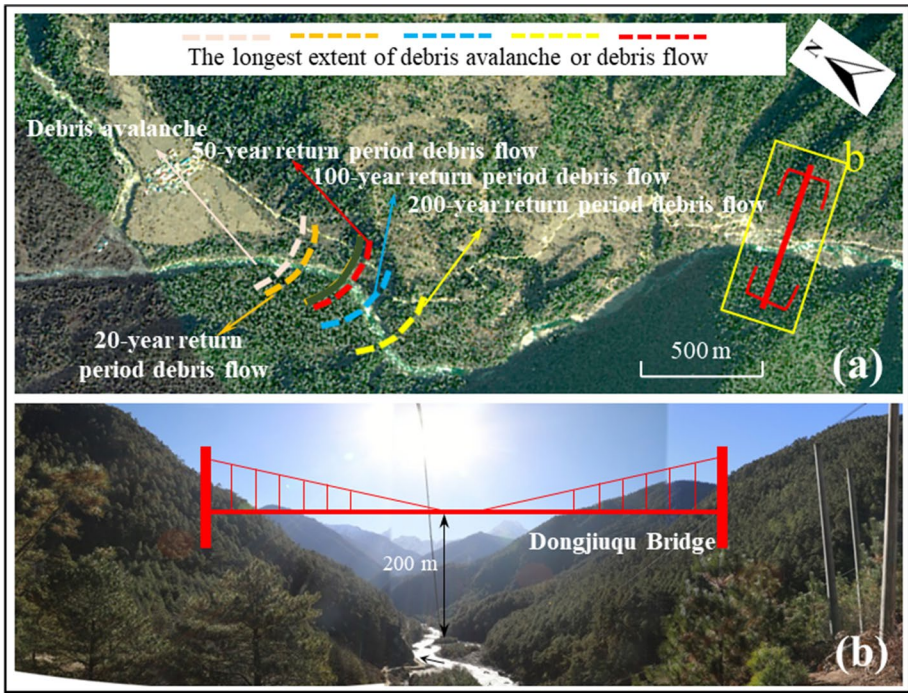


Fig. 17 a Relative position of debris avalanches and debris flows in different return periods with the proposed bridge, b the proposed bridge

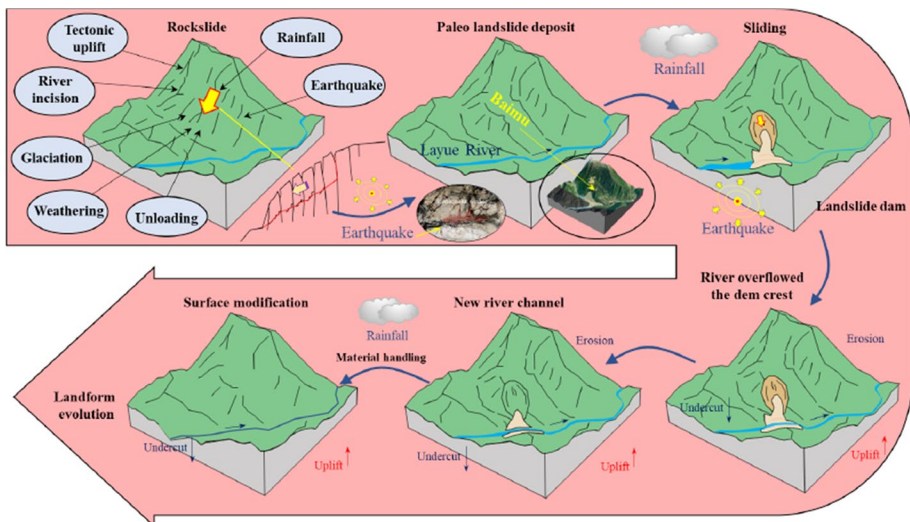


Fig. 18 Evolution sequence of formation and destruction of paleo deposits

margin of the Qinghai–Tibet Plateau (Fig. 18). Affected by strong regional tectonic activities, the Southeast margin of the Qinghai–Tibet Plateau is characterized by rapid topographic changes and frequent earthquakes, accompanied by strong rainfall, erosion, weathering, unloading, glacial activities and river undercutting. The bedrock in the source area of the Baimu deposit is steep and nearly parallel to the slope. Under the action of geological forces, bending deformation of rock mass is easy to occur producing tensile cracks. With the continuous expansion of deformation and cracks, the stability of the slope decreases. Finally, under the action of a strong earthquake, the slope is damaged and form a rock-slide (Fig. 18). The above genetic mechanism shows that in the Southeast margin of the Qinghai–Tibet Plateau, large-scale landslides are prone to occur under the synergistic effect of tectonic activities and climate, leading to the formation of a large number of Quaternary paleo deposits. These paleo-landslide deposits are easily reactivated under the influence of earthquakes and rainfall, resulting in landslides and river blocking. After the channel is blocked, the water level in the upstream of the dam will continue to rise and cause continuous erosion to the dam. This process may be short-term or long-term. This is related to topography, material composition of landslide dam and erosion capacity of river (Costa and Schuster 1988; Chen et al. 2018; Delaney and Evans 2015; Fan et al. 2020). The deep and narrow valleys in the Southeast margin of Qinghai–Tibet Plateau are especially favorable for landslide dams formation, and some blockages can exist for thousands of years (Fan et al. 2020). New river channels are formed under the continuous erosion of the river. The shape of the river is changed. After that, affected by river bed uplift and surface reconstruction, the evolution of regional river geomorphology will continue.

## 6 Conclusion

Safety of the Dongjiuqu Bridge—an important part of the Sichuan–Tibet Railway, must be ensured. Therefore, determining the stability of the Baimu paleo-landslide deposit and the scale of potential failure are of great significance. In this study, quantitative methods based on various numerical models are applied to solve different geological problems. The stability is evaluated using finite element analysis (the ABAQUS model). The development of the deformation zone is analyzed, and the safety factor of the potential failure zone is calculated to be 1.24. For the potential failure zone with a volume of  $1.1 \times 10^8 \text{ m}^3$ , the dynamic process of debris avalanche or debris flow that might occur is simulated using discrete element model and shallow water flow model. The results show that once the debris avalanche or debris flow occurs, most of it will accumulate at the mouth of the Baimu gully, and the minimum distance between the deposit and the proposed bridge is 1.6 km. Therefore, debris avalanche or debris flow will be no direct threat to the bridge. However, they can cause river blocking and form a lake in the Layue River more than 70 m deep, whose breach will cause an outburst flood. This disaster chain caused by the destruction of paleo deposits is a typical surface dynamic process on the Southeastern margin of the Qinghai–Tibet Plateau. Therefore, we propose the formation and evolution sequence of paleo deposits, which is of great significance to reflect the role of deposits on the evolution of local river geomorphology.

**Acknowledgements** This work was supported by the National Key Research and Development Plan (Grant No. 2018YFC1505301), the National Natural Science Foundation of China (Grant Nos. 41941017, U1702241). The authors would like to thank the editor and anonymous reviewers for their comments and suggestions which helped a lot in making this paper better.

## Declarations

**Conflict of interest** The authors declare that they have no known competing financial interests or personal relationships that could have appeared to influence the work reported in this paper.

## References

- Bao YD, Chen JP, Sun XH, Han XD, Li YC, Zhang YW, Gu FF, Wang JQ (2019a) Debris flow prediction and prevention in reservoir area based on finite volume type shallow-water model: a case study of pumped-storage hydroelectric power station site in Yi County, Hebei, China. *Environ Earth Sci* 78(19):1–16
- Bao YD, Han XD, Chen JP, Zhan JW, Zhang W, Sun XH, Chen MH (2019b) Numerical assessment of failure potential of a large mine waste dump in Panzhihua City, China. *Eng Geol* 253:171–183
- Bao YD, Zhai SJ, Chen JP, Xu PH, Sun XH, Zhan JW, Zhang W, Zhou X (2020) The evolution of the Samaoding paleo-landslide river blocking event at the upstream reaches of the Jinsha River, Tibetan Plateau. *Geomorphology* 351:106970
- Bishop AW (1973) The stability of tips and spoil heaps. *J Exp Biol* 6:1851–1861
- Bordoni M, Meisina C, Valentino R, Lu N, Bittelli M, Chersich S (2015) Hydrological factors affecting rainfall-induced shallow landslides: from the field monitoring to a simplified slope stability analysis. *Eng Geol* 193:19–37
- Borykov T, Mège D, Mangeney A, Richard P, Gurgurewicz J, Lucas A (2019) Empirical investigation of friction weakening of terrestrial and martian landslides using discrete element models. *Landslides* 16(6):1121–1140
- Capra L, Macias JL (2002) The cohesive Naranjo debris flow deposit (10 km<sup>3</sup>): a dam breakout flow derived from the Pleistocene debris-avalanche deposit of Nevado de Colima Volcano (Mexico). *J Volcanol Geothermal Res* 117:213–235
- Cascini L, Cuomo S, Pastor M, Rendina I (2016) SPH-FDM propagation and pore water pressure modelling for debris flows in flume tests. *Eng Geol* 213:74–83
- Chang M, Tang C, Van Asch ThWJ, Cai F (2017) Hazard assessment of debris flows in the Wenchuan earthquake-stricken area. *South West China Landslides* 14(5):1783–1792
- Chen HX, Zhang LM, Gao L, Yuan Q, Lu T, Xiang B, Zhuang WH (2017) Simulation of interactions among multiple debris flows. *Landslides* 14:595–615
- Chen J, Zhou W, Cui Z, Li W, Wu S, Ma J (2018) Formation process of a large paleo-landslide-dammed lake at Xuelongnang in the upper Jinsha River, SE Tibetan Plateau: constraints from OSL and 14C dating. *Landslides* 15:2399–2412
- Cheng ZL, Wu JS, Geng XY (2005) Debris flow dam formation in southeast Tibet. *J Mt Sci* 2(2):155–163
- Cheng ZL, Geng XY, Dang C, Liu JJ (2007) Modeling experiment of break of debris-flow dam. *Wuhan Univ J Nat Sci* 12(4):588–594
- Cheng ZL, Liu JJ, Liu JK (2010) Debris flow induced by glacial lake break in southeast Tibet. *WIT Trans Eng Sci* 67:101–111
- Cho YC, Song YS (2014) Deformation measurements and a stability analysis of the slope at a coal mine waste dump. *Ecol Eng* 68:189–199
- Costa JE, Schuster RL (1988) The formation and failure of natural dams. *Bull Geol Soc Am* 100:1054–1068
- Cui P, Chen XP, Wang YY, Hu KH, Li Y (2005) Jiangjia Ravine debris flows in the southwestern China. In: Jakob M, Hungr O (eds) *Debris-flow hazards and related phenomena*. Springer, Heidelberg, pp 565–594
- Cundall P, Strack O (1979) A discrete numerical model for granular assemblies. *Geotechnique* 29:47–65
- Cuomo S, Pastor M, Capobianco V, Cascini L (2016) Modelling the space-time evolution of bed entrainment for flow-like landslides. *Eng Geol* 212:10–20
- Dai Z, Huang Y (2016) A three-dimensional model for flow slides in municipal solid waste landfills using smoothed particle hydrodynamics. *Environ Earth Sci* 75:134
- Delaney KB, Evans SG (2015) The 2000 Yigong landslide (Tibetan Plateau), rockslide-dammed lake and outburst flood: Review, remote sensing analysis, and process modelling. *Geomorphology* 246:377–393
- Dufresne A, Geertsema M, Shugar DH, Koppes M et al (2018) Sedimentology and geomorphology of a large tsunamigenic landslide, Taan Fiord, Alaska. *Sed Geol* 364:302–318
- Falco MD, Crescenzo GD, Santo A (2012) Volume estimate of flow-type landslides along carbonatic and volcanic slopes in Campania (Southern Italy). *Nat Hazards* 61:51–63

- Fan X, Rossiter DG, Westen CJ, Xu Q, Görüm T (2015) Empirical prediction of coseismic landslide dam formation. *Earth Surf Process Landf* 39:1913–1926
- Fan XM, Dufresne A, Subramanian SS et al (2020) The formation and impact of landslide dams—State of the art. *Earth-Sci Rev* 203:103116
- Farah K, Ltifi M, Hassis H (2011) Reliability analysis of slope stability using stochastic finite element method. *Procedia Eng* 10:1402–1407
- Gan BR, Yang XG, Liao HM, Zhou ZW (2020) Flood routing process and high dam interception of natural discharge from the 2018 Baige Landslide-Dammed Lake. *Water* 12(2):605
- Gao Y, Li B, Gao HY, Chen LX, Wang YF (2020) Dynamic characteristics of high-elevation and long-runout landslides in the Emeishan basalt area: a case study of the Shuicheng “7.23” landslide in Guizhou, China. *Landslides* 17:1663–1677
- Geng BT (2015) Study on the stability of moraine landslides in the Palong Zangbo basin, southeastern Tibet. Southwest Petroleum University (in Chinese)
- Han XD, Chen JP, Xu PH, Zhan JW (2017) A well-balanced numerical scheme for debris flow run-out prediction in Xiaojia Gully considering different hydrological designs. *Landslides* 16:2105–2114
- Han XD, Chen JP, Xu PH, Niu CC, Zhan JW (2018) Runout analysis of a potential debris flow in the dongwopu gully based on a well-balanced numerical model over complex topography. *Bull Eng Geol Environ* 77:679–689
- Hu YX, Yu ZY, Zhou ZW (2020) Numerical simulation of landslide-generated waves during the 11 October 2018 Baige landslide at the Jinsha River. *Landslides*. <https://doi.org/10.1007/s10346-020-01382-x>
- Hurlimann M, Rickenmann D, Graf C (2003) Field and monitoring data of debris-flow events in the Swiss Alps. *Can Geotechn J* 40:161–175
- Itasca Consulting Group Inc (2008) PFC3D Particle Flow Code in 3 Dimensions, User’s Guide, Minneapolis
- Jarari NH, Stark TD, Merry S (2013) The July 10 2000 Payatas landfill slope failure. *Int J Geoenviron Geol* 2:208–228
- Khan MS, Hossain S, Ahmed A, Faysal M (2017) Investigation of a shallow slope failure on expansive clay in Texas. *Eng Geol* 219:118–129
- Li MH, Zhang L, Ding C, Li WL, Luo H, Liao MS, Xu Q (2020a) Retrieval of historical surface displacements of the Baige landslide from time-series SAR observations for retrospective analysis of the collapse event. *Remote Sens Environ* 240:111695
- Li R, Wang FW, Zhang S (2020b) Failure mechanism of a flow-like landslide triggered by the 2018 Western Shimane Earthquake. *Landslides*. <https://doi.org/10.1007/s10346-020-01401-x>
- Li YC, Chen JP, Li ZH, Han XD, Zhai SJ, Li YC, Zhang YW (2021a) A case study of debris flow risk assessment and hazard range prediction based on a neural network algorithm and finite volume shallow water flow model. *Environ Earth Sci* 80(7):275
- Li ZH, Wang Q, Zhou FJ et al (2021b) Integrating an interferometric synthetic aperture radar technique and numerical simulation to investigate the Tongmai old deposit along the Sichuan–Tibet Railway. *Geomorphology* 377:107586
- Liang QH (2010) Flood simulation using a well-balanced shallow flow model. *J Hydraul Eng* 136:669–675
- Lin CH, Lin ML (2015) Evolution of the large landslide induced by Typhoon Morakot: a case study in the Butangbanasi River, southern Taiwan using the discrete element method. *Eng Geol* 197:172–187
- Lin CW, Shieh CL, Yuan BD, Shieh YC, Liu SH, Lee SY (2003) Impact of Chi-Chi earthquake on the occurrence of landslides and debris flows: example from the Chenyulan River watershed, Nantou, Taiwan. *Eng Geol* 71:49–61
- Liu HD, Li DD, Wang ZF (2018) Dynamic process of the Wenjiagou rock landslide in Sichuan Province. *China Arab J Geosci* 11:233
- Lo CM, Lin ML, Tang CL, Hu JC (2011) A kinematic model of the Hsiaolin landslide calibrated to the morphology of the landslide deposit. *Eng Geol* 123:22–39
- Lu CY, Tang CL, Chan YC, Hu JC, Chi CC (2014) Forecasting landslide hazard by the 3D discrete element method: a case study of the unstable slope in the Lushan hot spring district, Central Taiwan. *Eng Geol* 183:14–30
- Medina V, Hurlimann M, Bateman A (2008) Application of FLATModel, a 2D finite volume code, to debris flows in the northeastern part of the Iberian Peninsula. *Landslides* 5(1):127–142
- Neupane R, Chen HY, Cao CR (2019) Review of moraine dam failure mechanism. *Geomat Nat Haz Risk* 10(1):1948–1966
- O’Brien JS (2006) FLO-2D User’s manual. FLO-2D Software, Inc., Nutrioso
- Ouyang CJ, He SM, Xu Q, Luo Y, Zhang WC (2013) A MacCormack-TVD finite difference method to simulate the mass flow in mountainous terrain with variable computational domain. *Comput Geosci* 52:1–10

- Ouyang C, He S, Tang C (2015a) Numerical analysis of dynamics of debris flow over erodible beds in Wenchuan earthquake-induced area. *Eng Geol* 194:62–72
- Ouyang C, He S, Xu Q (2015b) MacCormack-TVD finite difference solution for dam break hydraulics over erodible sediment beds. *J Hydraul Eng* 141:06014026
- Poisel R, Roth W (2004) Runout models of rock slope failures. *Felsbau* 22:46–50
- Poisel R, Bednarik M, Holzer R, Liščák P (2005) Geomechanics of hazardous landslides. *J Mt Sci* 2(3):211–217
- Potyondy DO, Cundall PA (2004) A bonded-particle model for rock. *Int J Rock Mech Min Sci* 41:1239–1364
- Shang YJ, Yang ZF, Li LH, Liu DA, Liao QL, Wang YC (2003) A super-large landslide in Tibet in 2000: background, occurrence, disaster, and origin. *Geomorphology* 54:225–243
- Shang YJ, Hyun CU, Park HD, Yang ZF, Yuan GX (2017) The 102 Landslide: human–slope interaction in SE Tibet over a 20-year period. *Environ Earth Sci* 76:47
- Specifications for Geological Investigation of Debris Flows Stabilization (DZ/T0220–2006) (2006) Published by the Ministry of Natural Resources of the People's Republic of China
- Spreafico MC, Francioni M, Cervi F et al (2016) Back analysis of the 2014 San Leo landslide using combined terrestrial laser scanning and 3D distinct element modelling. *Rock Mech Rock Eng* 49(6):2235–2251
- Steiakakis E, Kavouridis K, Monopolis D (2009) Large scale failure of the external waste dump at the “south Field” lignite mine, Northern Greece. *Eng Geol* 104:269–279
- Su WX, Miller HDS (1995) Waste pile stability and debris flow formation. The 35th U.S. Symposium on Rock Mechanics (USRMS), 5–7 June, Reno
- Tang CL, Hu JC, Lin ML, Angelier J, Lu CY, Chan YC, Chu HT (2009) The Tsaoling landslide triggered by the Chi-Chi earthquake, Taiwan: insights from a discrete element simulation. *Eng Geol* 106:1–19
- Tang CL, Hu JC, Lin ML, Yuan RM, Cheng CC (2013) The mechanism of the 1941 Tsaoling landslide, Taiwan: insight from a 2D discrete element simulation. *Environ Earth Sci* 70(3):1005–1019
- Technical code for building slope engineering (GB50330–2013) (2013) Published by the Ministry of Housing and Urban-Rural Development of the People's Republic of China and The State Administration for Market Regulation
- Wang GH, Wang YX, Lu WB, Zhou CB, Chen M, Peng Y (2015) XFEM based seismic potential failure mode analysis of concrete gravity dam–water–foundation system through incremental dynamic analysis. *Eng Struct* 98:81–94
- Waythomas CF (2001) Formation and failure of volcanic debris dams in the Chakachatna River valley associated with eruptions of the Spurr volcanic complex, Alaska. *Geomorphology* 39:111–129
- Xiao J, Gong W, Martin Ii JR, Shen M, Luo Z (2016) Probabilistic seismic stability analysis of slope at a given site in a specified exposure time. *Eng Geol* 212:53–62
- Yavari-Ramshe S, Ataie-Ashtiani B, Sanders BF (2015) A robust finite volume model to simulate granular flows. *Comput Geotech* 66:96–112
- Yin YP, Li B, Wang WP, Zhan LT, Xue Q, Gao Y, Zhang N, Chen HQ, Liu TK, Li AG (2016) Mechanism of the December 2015 catastrophic landslide at the Shenzhen landfill and controlling geotechnical risks of urbanization. *Engineering* 2:230–249
- Zheng H, Liu DF, Li CG (2005) Slope stability analysis based on elasto-plastic finite element method. *Int J Numer Methods Eng* 64:1871–1888
- Zhou JW, Huang KX, Shi C, Hao MH (2015) Discrete element modeling of the mass movement and loose material supplying the gully process of a debris avalanche in the Bayi Gully, Southwest China. *J Asian Earth Sci* 99:95–111
- Zhou JW, Cui P, Hao MH (2016) Comprehensive analyses of the initiation and entrainment processes of the 2000 Yigong catastrophic landslide in Tibet, China. *Landslides* 13:39–54
- Zhu CQ, Huang Y, Zhan LT (2018) SPH-based simulation of flow process of a landslide at Hongao landfill in China. *Nat Hazards* 93:1113–1126